

Original article

Adsorption and desorption characteristics of coal seam gas under infrared radiation

Yuying Tu¹, Yongli Zhang¹✉*, Yubin Dong², Yulin Ma¹

¹School of Mechanics and Engineering, Liaoning Technical University, Liaoning 123000, P. R. China

²School of Petroleum Engineering, China University of Petroleum, Beijing 102249, P. R. China

Keywords:

Desorption-induced hysteresis
infrared radiation
langmuir model
pressure sensitivity
desorption characteristics

Cited as:

Tu, Y., Zhang, Y., Dong, Y., Ma, Y.
Adsorption and desorption characteristics
of coal seam gas under infrared radiation.
Capillarity, 2023, 8(3): 53-64.
<https://doi.org/10.46690/capi.2023.09.02>

Abstract:

Infrared radiation technology can enhance rock permeability and promote methane desorption in coalbed methane thermal recovery. In this study, an experimental system with infrared radiation is developed to investigate the adsorption/desorption behavior of coal under different water contents. The results demonstrate that higher power levels of infrared radiation lead to decreased adsorption capacity and increased desorption capacity in coal. Specifically, employing 50 W infrared radiation results in a 30.9% increase in desorption capacity. Higher moisture content intensifies the desorption hysteresis effect, while this adverse impact can be mitigated by infrared radiation with greater power levels, exhibiting a stronger ability to reduce desorption-induced hysteresis. Additionally, a critical pressure for infrared radiation is established. Before and after this pressure, the influence of infrared radiation power on pressure sensitivity differs significantly. Finally, an improved Langmuir adsorption model considering infrared radiation power and moisture content is proposed and validated using experimental data. Our research expands the application of infrared radiation technology for enhanced coalbed methane recovery during actual mining operations.

1. Introduction

With the ongoing worldwide progress in pursuing carbon neutrality goals and achieving peak carbon dioxide emissions, the global energy structure is gradually changing in the direction of low-carbon technologies (Aylin and Tayfun, 2010; Feng and Zhang, 2012). China has abundant reserves of coalbed methane and a massive potential for exploitation. The efficient extraction of coalbed methane can promote the energy structure reform on the supply side and reduce instances of gas outbursts to ensure safe production in coal mines (Sang et al., 2010; Teng et al., 2017). The extraction of coalbed methane is negatively influenced by low pressure, permeability and porosity, as well as the high capacity of the reservoir for adsorption. The current mining technology is unsuitable for the large-scale underground extraction of coalbed methane (Lin et al., 2017; Fan et al., 2021; Guo et al., 2021a; Ye et al., 2021).

Therefore, it is essential to develop new technologies for mining coalbed methane (Guo et al., 2021b).

Several methods have been implemented to enhance coalbed methane mining and increase reservoir permeability, including fracturing-based stimulation, heat injection-based stimulation, and multi-gas displacement technology (Lu et al., 2021). However, none of these technologies can be effectively promoted. For example, although fracturing-based inspiration can expand the fracture network in a reservoir, it is limited by the mechanism of migration of the proppant as well as issues with the reverse drainage and treatment of the fracturing fluid (Avner et al., 2014; Yan et al., 2015; Liu et al., 2020). The permeability of the coal reservoir significantly influences gas displacement in the context of mining, and the displacement of CO₂ increases the risk of gas outbursts before CH₄ has been completely desorbed (Teng et al., 2016; Cai et al., 2019). Thermal injection-based mining can increase the

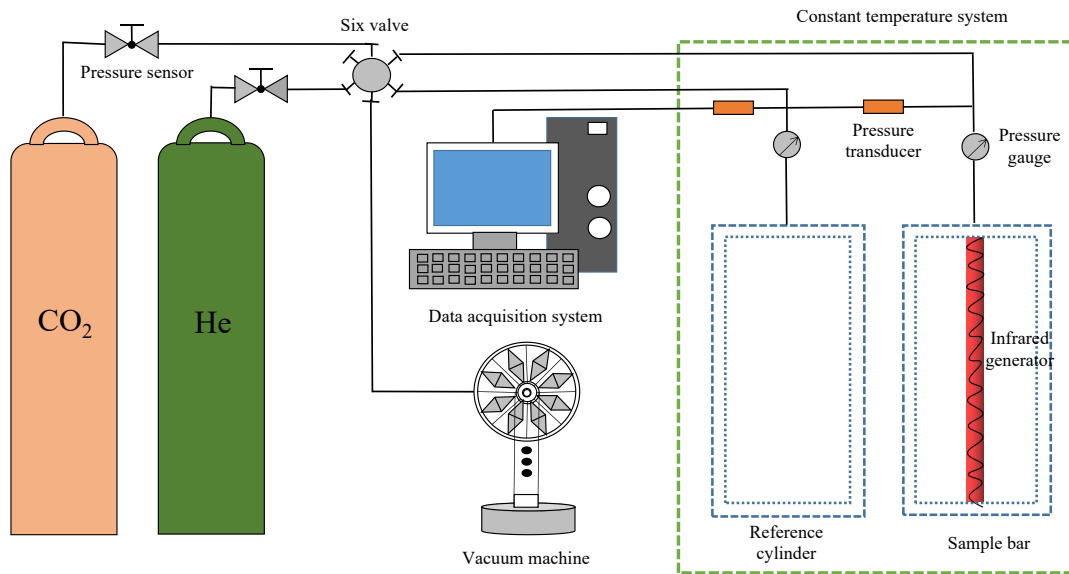


Fig. 1. The experimental system of this study.

desorption and migration of gas molecules to increase production via energy transfer; however, the corresponding increase in temperature may cause the expansion of the reservoir matrix and reduce permeability (Liu et al., 2022; Su et al., 2022).

The infrared radiation-based stimulation technology studied in this paper is heat injection-based stimulation. Infrared radiation can increase the temperature of the reservoir due to energy transfer while exhibiting the nature of electromagnetic waves. This heating method is characterized by fast heating speed, small thermal inertia, selective heating, intense penetration, and manageable control. Moreover, it can induce cracks in the reservoir, which is an improvement over traditional heat injection technology. Many scholars derived the key factors influencing the efficiency of infrared radiation by conducting heating experiments on thermoplastic materials (Jamil et al., 2015; Wang et al., 2015; Yu et al., 2016; Lan et al., 2020; Längauer et al., 2021). They compared the drying effects of infrared radiation-based heating and natural convection, and the results showed that the coefficient of mass transfer under infrared radiation is over ten times higher than that under natural convection. Infrared radiation-based heating technology has been widely used in the food, manufacturing and medical industries due to its advantages of low energy consumption, environmental friendliness and high heat transfer rate (Noboru and Tamotsu, 1994; Tomone et al., 2005; Salam et al., 2019).

In this paper, adsorption/desorption experiments using infrared radiation are conducted to explore the adsorption/desorption characteristics under the combined effects of radiation power, water content and pressure, and the key factors affecting the desorption performance of coal are evaluated. At the same time, the Langmuir isothermal adsorption model is modified at the theoretical level. This work enriches the theory and application of infrared radiation-based heating technology and expands the use of heat injection and electromagnetic stimulation to increase production. Compared to other coalbed

methane thermal recovery technologies, this technology is environmentally friendly and is expected to promote efficient technologies for mining coalbed methane.

2. Experiments

2.1 Sample collection and preparation

Raw coal was taken from the Wulong Mine in Fuxin, Liaoning Province, China. The mining area is located in the Fuxin Basin in the Yanliaotai fold belt, east of the China-Korea platform and south of Inner Mongolia. The primary structure consists of edge faults on the east and west sides of the basin, and the secondary structure mainly contains folds. The coal reservoir is characterized by soft texture, poor bearing capacity and low permeability (Xu et al., 2020; Song and Yao, 2022). The coal rock was collected from a recently exposed mining face and was crushed using a jaw crusher. The pulverized coal particles with a size of 0.25-0.18 mm were screened for subsequent use. The original coal rock was industrially analyzed, with the following results: Moisture content is 3.42; Ash ratio is 17.43; Volatile fraction is 37.17; Fixed carbon ratio is 41.98.

2.2 Experimental devices

An experimental system was developed to investigate the adsorption/desorption of coal rock under infrared radiation, which consists of infrared radiation, data acquisition, and pressure supply parts. The experimental system had suitable tightness and pressure resistance. A schematic diagram of the experimental device with infrared radiation to examine the adsorption/desorption of coal is shown in Fig. 1.

Compared with the traditional experimental setup used for the adsorption/desorption of coal rock, the practical device used herein was improved by adding an infrared radiation system and replacing CH_4 with CO_2 . On the one hand, infrared radiation can rapidly heat the coal rock, thus CH_4 should

not be used as the gas for adsorption under high temperature and pressure. CO₂, which has similar physical and chemical properties, should be applied instead as the gas for adsorption to ensure the safety and operability of the experiment. On the other hand, CO₂ adsorbs better in coal rock than CH₄ and thus can help widen the scope of application of infrared radiation-based stimulation technology to decomposition in cases where desorption is challenging (Krooss et al., 2002; Stefan et al., 2008; Boleslav, 2011).

2.3 Experimental scheme and steps

The moisture content of coal samples significantly influences adsorption/desorption; therefore, it is necessary to measure the equilibrium moisture level of coal samples before the experiment. After pre-wetting, the coal sample was placed into a constant-temperature drying oven for 48h together with the supersaturated potassium sulfate solution, where the calculated equilibrium moisture is:

$$M_e = \frac{G_1}{G_2} \times M_{ad} + \frac{G_2 - G_1}{G_2} \times 100 \quad (1)$$

where M_e represents the equilibrium moisture content of the sample, %; G_1 represents the mass of the air-dried sample before attaining equilibrium, g; G_2 represents the mass of the sample after attaining moisture equilibrium, g; and M_{ad} is its moisture content, %.

The samples were divided into four groups with different moisture contents and adsorption pressures (1-8 MPa). An experimental scheme was designed to assess the characteristics of adsorption/desorption under the action of infrared radiation, which included the following steps:

- 1) Weigh the pulverized coal and then deposit it into the sample cylinder. Pressurize the system with helium gas to a level of 1 MPa above the maximum adsorption pressure. Maintain this elevated pressure for a duration of 6 hours to validate the airtightness of the device. Evacuate the system and determine the volume of available free space. At the same time, open the helium valve on the reference cylinder and record its pressure. Proceed by opening the valve that connects the sample and reference cylinders and record the equilibrium pressure. Utilize the gas compression factor equation to calculate the volume of free space within the sample cylinder:

$$\begin{cases} \frac{P_1 V_1 T_1 T_2 Z_2 Z_3 + P_2 V_2 T T_1 Z_1 Z_3 + P_3 V_3 T_1 T_2 Z_1 Z_2}{Z_3 T (P_2 Z_1 T_1 - P_1 Z_2 T_2)} \\ V_f = V_0 - V_s \end{cases} \quad (2)$$

where V_s represents the volume of the sample, cm³; V_f represents the volume of free space, cm³; V_0 represents the total volume of the sample cylinder, cm³; P_1 , P_2 , and P_3 represent the equilibrium pressure, the initial pressure of the reference cylinder, and the initial pressure of the sample cylinder, respectively, MPa, where the data were collected separately through pressure sensors; T_1 , T_2 and T_3 represent their corresponding temperatures, respectively, K, where the data were collected separately through temperature sensors; V_1 , V_2 and V_3 represent the

volumes of the overall system, the reference cylinder, and the sample cylinder, respectively, cm³; Z_1 , Z_2 and Z_3 represent the compression factors of the gas after equilibrium, the initial compression factors of the reference cylinder, and the sample cylinder, respectively.

- 2) Activate the constant-temperature system and the infrared generator, convert the system into a vacuum by removing air, and then initiate the experiment on pressurization-induced adsorption. Once the reference cylinder has been filled with CO₂ at a certain pressure, open the valve between the reference cylinder and the sample cylinder and record the equilibrium pressure. Once adsorption has progressed to saturation, record the pressure, gradually increase the adsorption pressure, and repeat the above steps.
- 3) Once adsorption is complete, experiment on depressurization-induced desorption. Release the pressure of gases in the reference cylinder, open the valve between the cylinders and record the equilibrium pressure, record the desorbed pressure once again after desorption has been completed, gradually reduce the stress, and repeat the above steps. The capacity of the coal sample for adsorption at each pressure point can be obtained by the following formula:

$$\begin{cases} PV = nZRT \\ n_i = n_1 - n_2 \\ V_i = n_i \times 22.4 \times 1000 \\ V_{ad} = \frac{V_i}{G} \end{cases} \quad (3)$$

where P represents the pressure of the gas, MPa; V represents volume, cm³; n represents the number of moles, mol; Z is compression factor (a constant); R represents the molar constant of the gas, J/mol/K; T is temperature, K; n_1 represents the number of moles of the gas in the sample cylinder before the pressure points have been balanced, mol; n_2 represents the number of moles of the gas in the sample cylinder after each pressure point has been balanced, mol; n_i represents the number of moles of gas adsorbed by the coal sample, mol; V_i represents the volume of the adsorbed gas at each pressure point, cm³; V_{ad} represents the capacity of the coal sample to adsorb gas at each pressure point, cm³/g; and G represents the quality of the coal sample, g.

3. Results and discussion

3.1 Adsorption capacity

As shown in Fig. 2, the capacity of the coal samples for adsorption in each range of moisture content increases with pressure, first rising quickly and then slowing down. When the range of moisture content in coal samples is the same, their adsorption capacity decreases with the increase in the power of infrared radiation. This is because a higher power of infrared radiation increases the temperature of the coal sample, and gas molecules with higher energy are adsorbed in coal. The higher activity reduces the capacity of coal for adsorption.

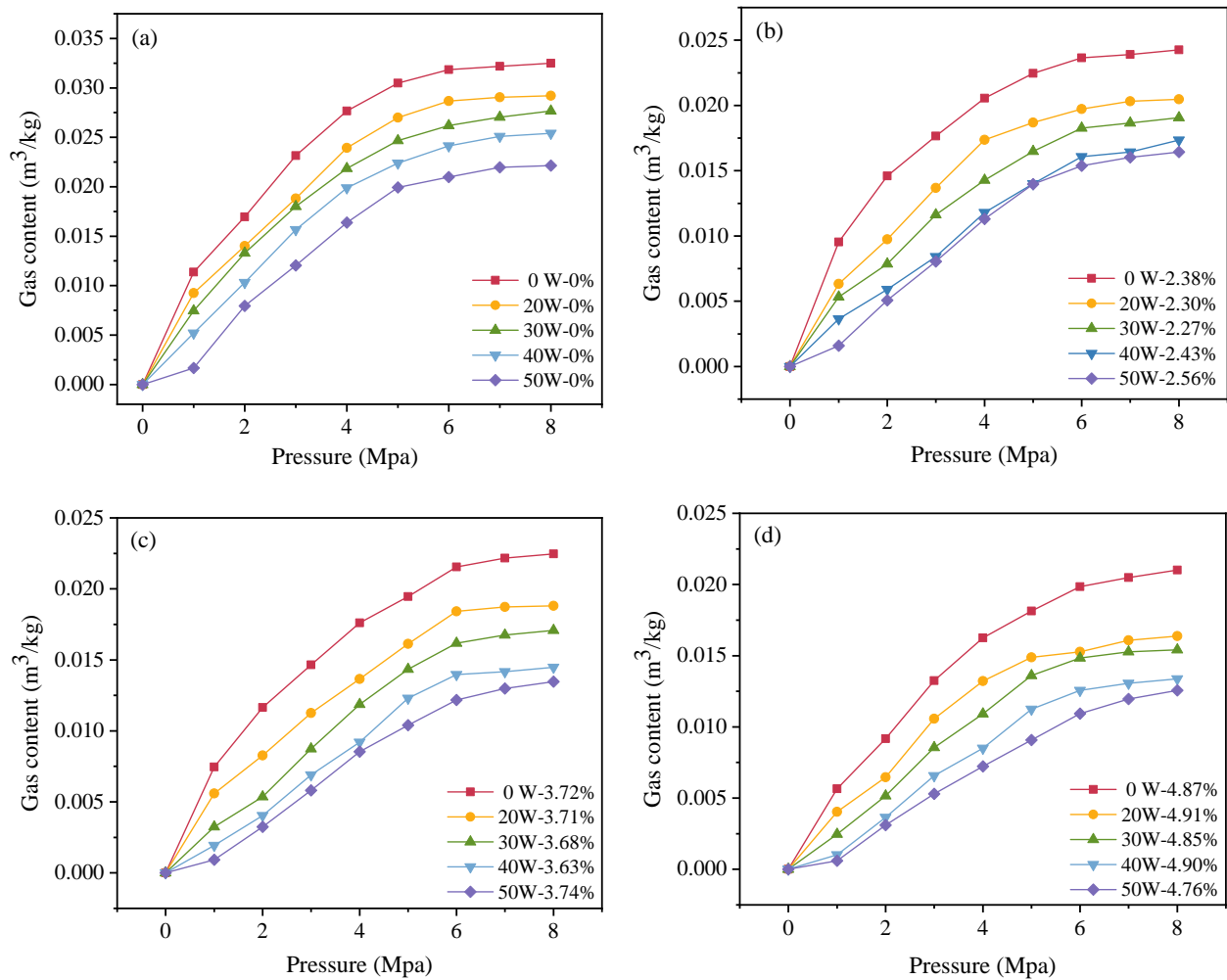


Fig. 2. Adsorption of coal samples with different moisture contents. (a) Moisture content, 0, (b) moisture content, 2%-3%, (c) moisture content, 3%-4%, (d) moisture content, 4%-5%.

For example, the adsorption capacity of coal samples with moisture content ranging from 3% to 4% is 0.0188 m³/kg when the radiation power is 20 W and the pressure is 8 MPa. When the intensity of infrared radiation is 50 W, the capacity of the sample for adsorption under the same force is only 0.0127 m³/kg. For coal samples with the same power of infrared radiation and different ranges of water content, the higher the water content, the lower their adsorption capacity. This is because coal has a higher affinity for water than CO₂, CH₄ and other gases (Wang et al., 2018). Therefore, a higher water content reduces the capacity of samples for coal adsorption. The experimental data demonstrate that under the action of infrared radiation with the same amplitude of change, the higher the water content of coal rock, the smaller the reduction in adsorption capacity; the reason is that when the internal water temperature increases, this reduces the molecular energy of coalbed methane.

3.2 Desorption volume

The broken-line diagram in Fig. 3 shows the desorption curves of coal samples with different moisture contents, with

the samples subjected to varying powers of infrared radiation. The histogram shows the desorption volume in the 1-8 MPa pressure field during depressurization-induced desorption. This indicates that the desorption curves of coal samples with the same range of water content exhibit roughly the same trend of change as that of their adsorption curves with a rise in pressure under the same radiation power. The higher the radiation power, the smaller the content of the remaining gas in coal, and the more complete the desorption. For example, the coal sample with 0 water content has 0.0167 m³/kg of gas remaining after desorption at room temperature, while the remaining gas content of the coal sample with the same water content after desorption is 0.005 m³/kg after subjecting it to 50 W of infrared radiation. A histogram analysis reveals that a higher radiation power leads to a larger desorption volume in coal samples with different water content ranges during depressurization-induced desorption. To sum up, when the water content range is the same across samples, infrared radiation with a higher power reduces the volume of adsorption and increases that of desorption. Moreover, under the same power of infrared radiation, higher moisture content in the coal

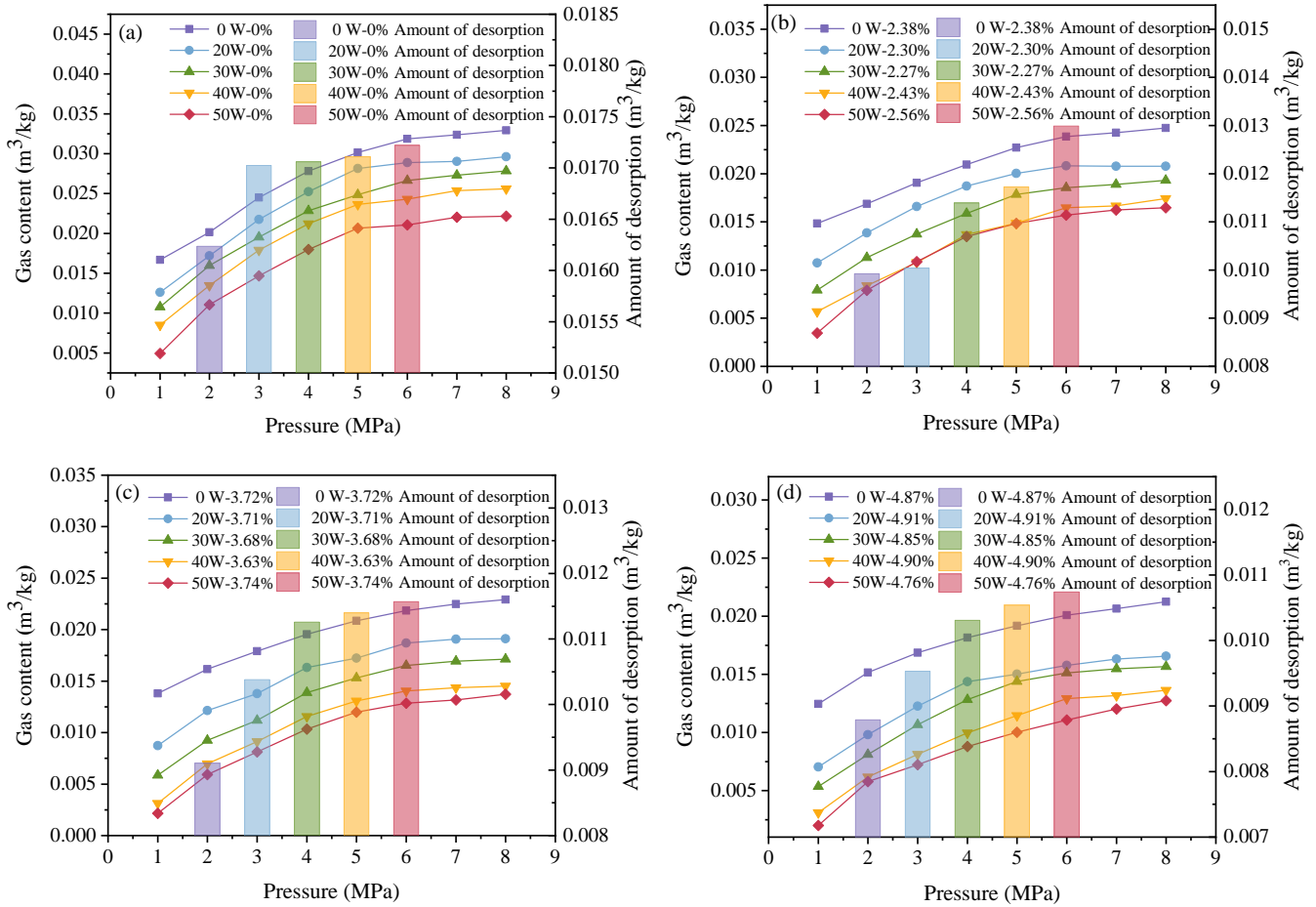


Fig. 3. Desorption of coal samples with different ranges of moisture content. (a) Moisture content, 0, (b) moisture content, 2%-3%, (c) moisture content, 3%-4%, (d) moisture content, 4%-5%.

samples leads to smaller volumes of adsorption and desorption, and through the calculation of desorption rate, it can be seen that the decrease in desorption is mainly due to the preferential adsorption of water by coal and the rock matrix.

3.3 Desorption lag

The upper surface in Fig. 4 represents the gas contents of coal samples with different water contents during desorption under external powers of infrared radiation. The lower surface represents the gas contents of coal samples under the same conditions during adsorption. The curve of desorption is always slightly higher than that of adsorption, and the interval between them becomes more prominent with a decrease in pressure.

When comparing coal samples with the same water content but different radiation power, as the radiation power increases, the adsorption and desorption curves are close, reflecting the relationship between the lag caused by desorption and the temperature of coal samples. The higher the temperature, the smaller the desorption-induced hysteresis, which is consistent with the results of previous research (Chen et al., 2021). In addition, compared with coal samples with different water contents before infrared radiation, it is found that the hysteresis

of desorption induction is enhanced with the increase in water content, and the hysteresis of moisture and desorption induction is the same, but it is weakened after infrared radiation. At the radiation power of 50 W, the desorption-induced hysteresis of all coal samples with four ranges of water content tends to be the same. Infrared radiation has a more significant effect in reducing desorption-induced hysteresis than the moisture content. If desorption-induced hysteresis can be reduced, the desorption volume of coal samples approaches that of their adsorption under the same conditions. Thus, their capacity for desorption is enhanced.

3.4 Pressure sensitivity

In order to analyze the response of desorption amount to pressure, radiation power and moisture, the effects of different radiation power and moisture content on the desorption amount of coal samples under reduced pressure are studied. To this end, the coefficient of sensitivity to pressure C_p is introduced. A higher value of this coefficient indicates that the volume of desorption is more sensitive to pressure under infrared radiation and in the presence of moisture. The desorption curves reflect a significant change in the desorption volume of samples, as:

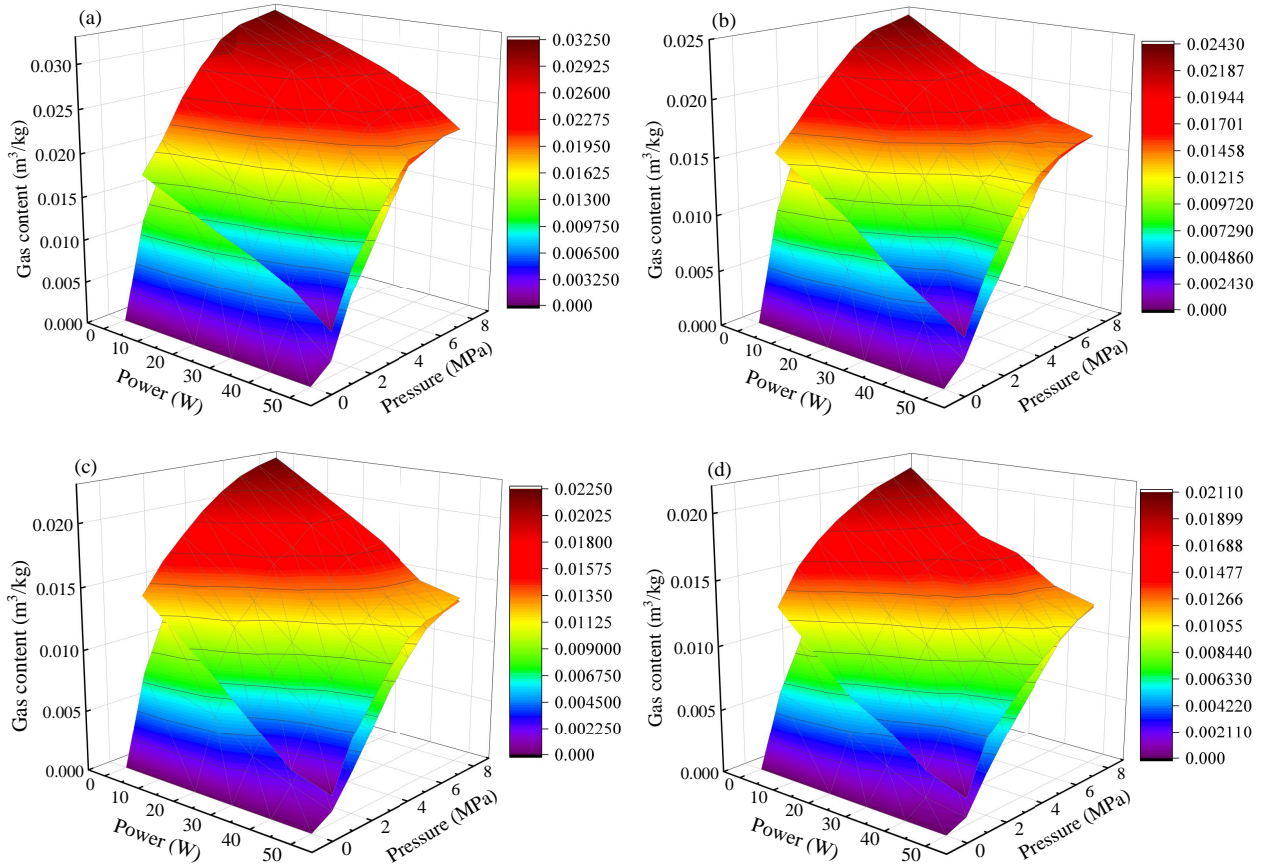


Fig. 4. Comparison of adsorption/desorption results for coal samples with different moisture contents. (a) Moisture content, 0, (b) moisture content, 2%-3%, (c) moisture content, 3%-4%, (d) moisture content, 4%-5%.

$$C_p = \frac{\partial V}{\partial P} \quad (4)$$

where C_p represents the pressure sensitivity of desorption, $\text{m}^3/(\text{kg}\cdot\text{MPa})$; ∂V represents the change in adsorption capacity, m^3/kg ; ∂P represents the change in pressure, MPa.

It is clear from Fig. 5 that as the pressure increases, the sensitivity of the capacity of coal sample for desorption to pressure decreases in the form of a power function, and the sensitivity of the same selection varies significantly under different radiation power when the pressure is low. With the increase in pressure, the difference in the sensitivity of the sample to pressure under different levels of infrared radiation gradually decreases. With the increase in pressure, there is a point of intersection in the curve of the sensitivity of desorption of the samples to different radiation levels. This shifts to the low-pressure area with the increase in the water content of coal samples. The higher the power of infrared radiation, the lower the sensitivity of desorption of the samples to pressure on the left side of the intersection. However, this relation is the opposite on the right side of the intersection. When the pressure on the coal sample is low, the degree of compression of the coal matrix is small and the internal channel for the migration of gas is unobstructed. Particles of the matrix expand under the action of infrared radiation and compress the pores in it. Such expansion-induced extrusion is

directly proportional to the power of infrared radiation, and the effect of changes in pressure on the desorption and migration of gas is less prominent than that on coal samples not subjected to infrared radiation. The pressure is higher in the area on the right side of the intersection, the coal sample is significantly compressed, and its internal pores and cracks are squeezed. Infrared radiation leads to a difference in temperature within the coal sample that results in a “thermal tearing” effect, and new cracks are formed in it. The gas still moves in the channel at high pressure. The capabilities of desorption and migration are still responsive to pressure, so in the high-pressure area on the right side of the intersection, the pressure sensitivity of coal samples under high power of infrared radiation is higher than that of coal samples under low power of infrared radiation. The data on the sensitivity of the capacity for desorption to pressure is fitted as $C_p = \alpha_p P^{-\beta}$. The results are adequate with $R^2 > 0.95$. The analysis of the parameters of fitting reveal that the parameters α_p and β decrease with an increase in the power of infrared radiation and the moisture content.

4. Model establishment and validation

The Langmuir model of isothermal adsorption is often used to quantitatively assess the capacity of coal rock for adsorption. However, this model is not applicable when the effects of the environmental temperature and water content are

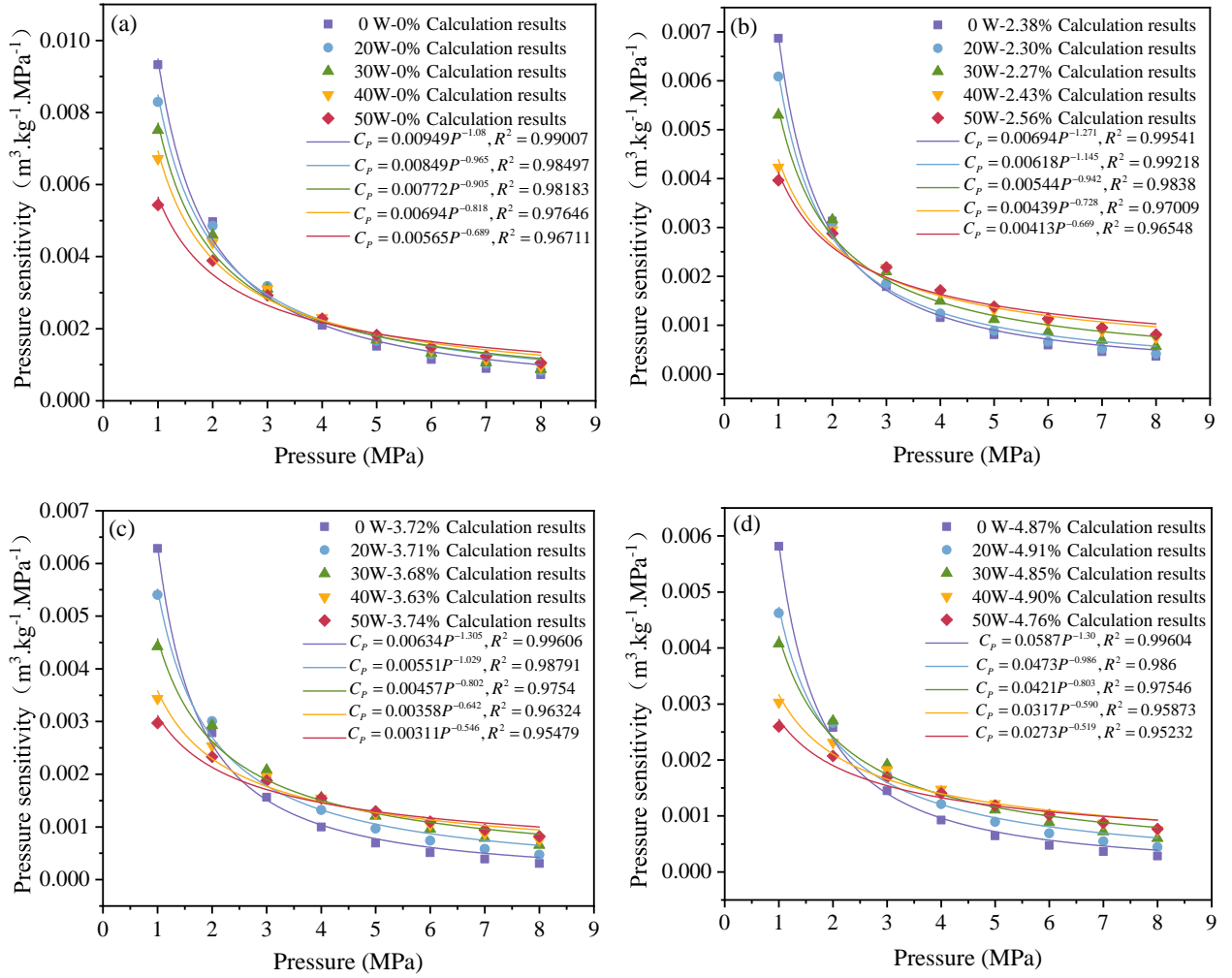


Fig. 5. Sensitivity of the desorption capacity to pressure. (a) Moisture content, 0, (b) moisture content, 2%-3%, (c) moisture content, 3%-4%, (d) moisture content, 4%-5%.

considered (Qin et al., 2022). Therefore, the Langmuir model of isothermal adsorption is modified as follows:

$$V_p = \frac{abp}{1 + bp} \quad (5)$$

where V_p represents the volume of adsorption of the coal sample when the adsorption pressure is p , m³/kg; a represents the maximum capacity of the coal sample for adsorption, m³/kg; b represents the comprehensive Langmuir parameters in terms of the ratio of the rate of adsorption to that of desorption, and p represents the adsorption pressure, MPa.

The above parameters are related to the adsorption-induced heat and the temperature of the coal sample (Ye et al., 2016; Laith et al., 2020):

$$b = \frac{\alpha}{k_{dn}\sqrt{2\pi MR_g T}} \exp\left(\frac{Q}{R_g T}\right) \quad (6)$$

where α represents the coefficient of viscosity, Pa·s; k_{dn} represents the constant of the rate of desorption at an infinite temperature; M represents the molecular weight of the adsorbed gas, g/mol; R_g is a gas constant, J/(kg·K); Q represents

the absorbed heat, J.

The relationship between the capacities of water-bearing coal samples and dry coal samples for adsorption can be expressed as (Chen et al., 2012):

$$V_w = V_d \exp(-\lambda m) \quad (7)$$

where V_w represents the capacity of the gas for adsorption in the water-bearing coal sample per unit mass, cm³/kg; V_d is the same but for dry coal per unit mass, cm³/kg; λ represents the coefficient of reduction in the adsorption of coal rock; and m is the moisture content.

Simplifying Eqs. (5)-(7) obtains the improved Langmuir equation of adsorption that considers the influence of temperature and moisture V_{T-w} :

$$V_{T-w} = \frac{\alpha a P \exp\left(\frac{Q}{R_g T} - \lambda m\right)}{k_{dn}\sqrt{2\pi MR_g T} + \alpha P \exp\left(\frac{Q}{R_g T}\right)} \quad (8)$$

To intuitively and accurately explore changes in the temperature of the coal samples under the action of infrared radiation, the temperature T in the improved equation of adsorption was

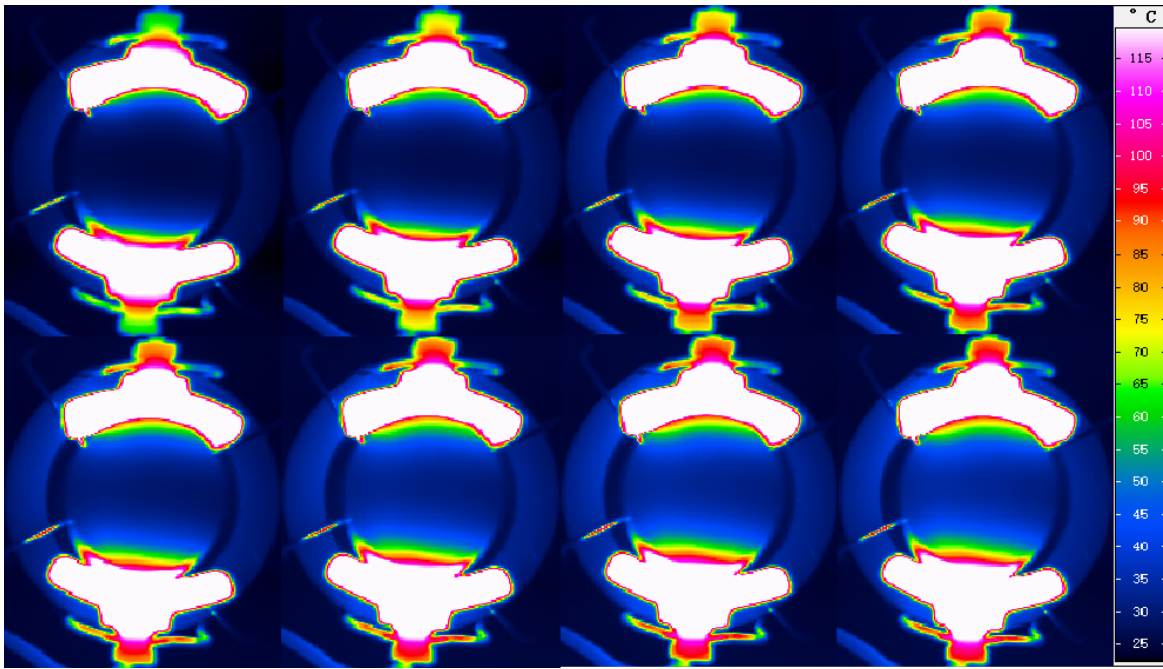


Fig. 6. Results of the thermal imaging of changes in the temperature of coal samples under infrared radiation.

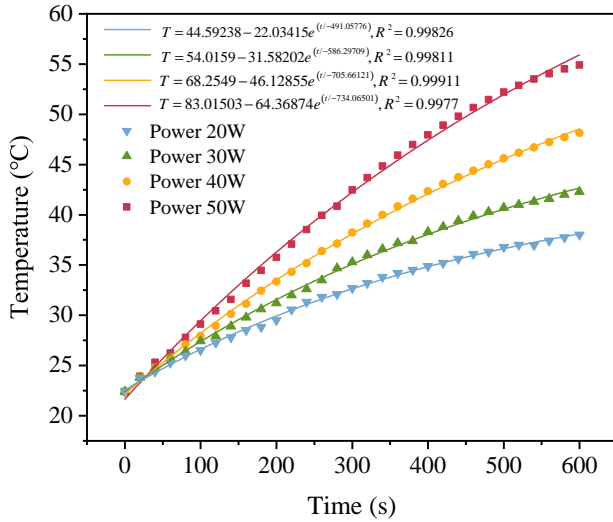


Fig. 7. Changes in the temperature of coal samples subjected to different levels of infrared radiation.

determined by the power and duration of application of infrared radiation; an experiment was designed to this end. This uses an infrared ceramic-plate heater (radiation wavelength, 2-10 μm ; rated radiation power, 100 W) as the source of radiation. Its working current is controlled by providing external resistance such that the radiation power is the same as in the adsorption/desorption experiments. An infrared thermal imager is employed to monitor the temperature of the coal samples in real time (as shown in Fig. 6). A thermal imaging analysis software is implemented to select the coal samples, the average temperatures of which are calculated under different radiation powers.

Fig. 7 shows the changes in the average temperature of coal samples under different radiation levels as calculated by

the IRBIS thermal imaging analysis software. The average temperature of samples increase gradually with the duration of application of radiation. The more the power of infrared radiation, the higher the temperature of the sample during the prescribed duration of radiation. However, regardless of the radiation power used, the overall temperature of the coal samples exhibits a trend of quickly rising and then slowing down. The results of fitting the data into $T = T_0 + Ae^{t/t_0}$ are satisfactory, with a value of R^2 higher than 0.99. T_0 , $|A|$, and $|t_0|$ exhibit an increasing trend with the power of infrared radiation.

The increasing trend in temperature shows that as the duration of radiation increases, the temperature of the coal sample tends toward a stable value, which is in the fitting formula. Because the adsorption/desorption process takes a long time, the coal sample reaches its highest temperature in this process. The maximum temperatures under different powers of infrared radiation are fitted, and the results are shown in Fig. 8. The relationship between the maximum temperature and radiation power was derived using this approach:

$$T = 22.4 + 1.15878w \quad (9)$$

where w is infrared radiation power, W. The above experiment also yielded the relationship between the temperature of coal sample and the power and duration of radiation. The three-dimensional fitting surface is shown in Fig. 9 This provides a theoretical reference for controlling the temperature of coal rock under the action of infrared radiation:

$$T = 461.92 - \frac{503.76363}{1 + \left(\frac{t+153.14807}{477.39371}\right)^2} - \frac{421.82755}{1 + \left(\frac{w-0.41913}{178.12655}\right)^2} + \frac{485.61657}{\left(\frac{t+153.14807}{477.39371}\right)^2 \left(\frac{w-0.41913}{178.12655}\right)^2} \quad (10)$$

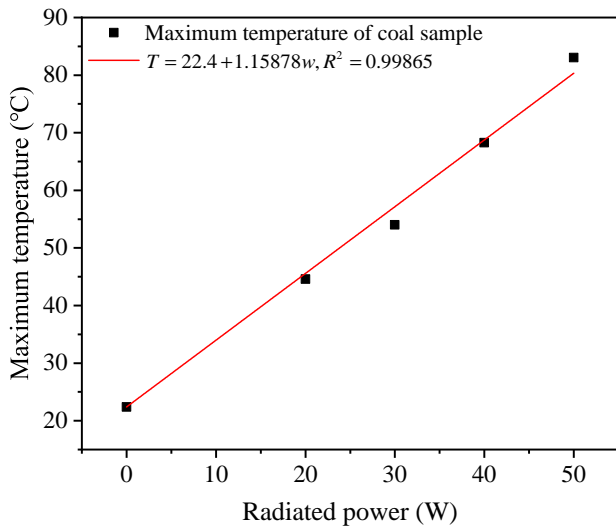


Fig. 8. Maximum temperature of coal samples subjected to radiation.

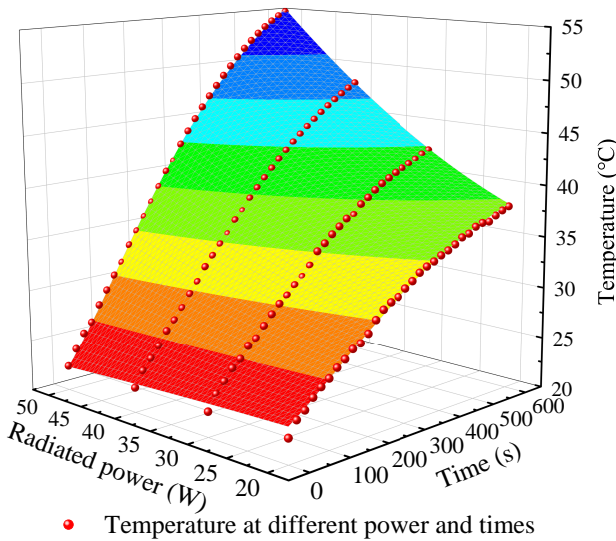


Fig. 9. Three-dimensional fitting surfaces for temperature, power and time.

The improved Langmuir model of adsorption is combined with Eqs. (8) and (9) as follows:

$$V_{T-w} = \frac{\alpha a P \exp \left[\frac{Q}{R_g(22.4 + 1.15878w)} - \lambda m \right]}{k_{dn} \sqrt{2\pi M R_g(22.4 + 1.15878w)} + \alpha P \exp \left[\frac{Q}{R_g(22.4 + 1.15878w)} \right]} \quad (11)$$

The improved Langmuir equation can fit the data on desorption for the coal samples under infrared radiation, and the results are shown in Fig. 10 and Table 1.

It is intuitively clear that the value of R^2 is above 0.95, which indicates that the effect of fitting is good. An analysis of the maximum adsorption capacity, a , shows that its value gradually decreases with an increase in the radiation power for coal samples with the same range of water content. For example, for samples with water content ranging from 2% to

3%, at room temperature, an a value of $0.0358 \text{ m}^3/\text{kg}$ was recorded, which was $0.0311 \text{ m}^3/\text{kg}$ when the power was 20 W, and $0.0287 \text{ m}^3/\text{kg}$ when the radiation power was 50 W. This indicates that the power of infrared radiation can inhibit adsorption by the coal samples. The higher the power of infrared radiation, the lower the maximum capacity of samples for adsorption, which is consistent with previous experimental conclusions. The results of fitting of samples with different water contents under the same power of infrared radiation show that the higher the water content, the smaller the value of a . When the radiation power was 40 W, the value of a of samples with 0 water content was $0.0373 \text{ m}^3/\text{kg}$, which was $0.0291 \text{ m}^3/\text{kg}$ for samples with a water content of 2.43%, and $0.0264 \text{ m}^3/\text{kg}$ for samples with a water content of 4.90%. These results indicate that moisture also inhibits the capacity of coal samples for adsorption, and the higher the water content, the lower the adsorption capacity.

5. Conclusions

In this work, to comprehensively investigate the adsorption and desorption processes in coal rock samples with varying moisture content, we conducted a series of quantitative experiments where samples were subjected to infrared radiation. The following conclusions were obtained:

- 1) Both the infrared radiation and the water content inhibit adsorption to the coal rock during pressurized adsorption. The higher the power of the infrared radiation and the higher the water content, the lower the capacity of the coal samples for adsorption at the same pressure. In the process of step-down desorption, the more complete the desorption of coal samples under high power of infrared radiation and water content, and the higher the power of infrared radiation, the greater the volume of desorption under the same water content. Moreover, under the same infrared radiation power, the higher the water content, the smaller the volume of desorption. These results show that infrared radiation helps increase desorption from coal rock and plays a leading role in gas desorption from water-bearing coal samples.
- 2) The processes of desorption and adsorption are not entirely reversible. As the desorption-induced pressure decreases, the difference between the curves of desorption and adsorption increases, that is, the lag in desorption gradually enlarges. Infrared radiation reduces this lag along with the water content, thus increasing the desorption yield; the higher the power of infrared radiation, the higher the desorption.
- 3) As the desorption-induced pressure increases, the sensitivity of desorption to pressure gradually diminishes, and the sensitivity curves feature a point of intersection that gradually shifts to low pressure with increasing water content. The main factor influencing the pressure sensitivity of desorption on the left side of the intersection is the thermal expansion of the coal particles under the action of infrared radiation. The initially smooth channel for the migration of gas is affected by the expansion of the coal matrix, whereas this renders the capacity for

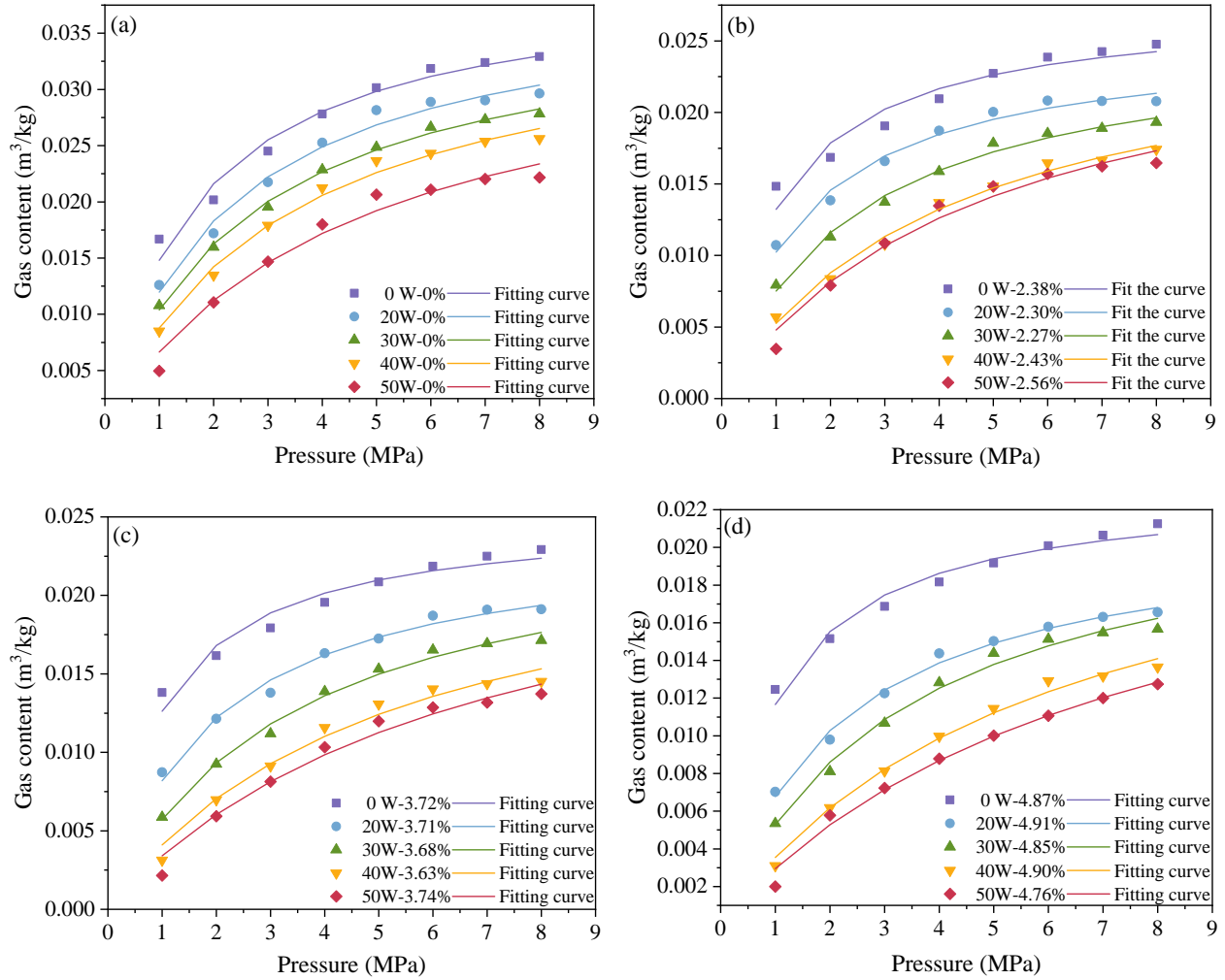


Fig. 10. Results of fitting of improved Langmuir model of adsorption. (a) Moisture content, 0, (b) moisture content, 2%-3%, (c) moisture content, 3%-4%, (d) moisture content, 4%-5%.

Table 1. Fitting parameters of improved Langmuir equation under different water contents and radiation levels.

Moisture content	Power	a	R^2	Moisture content	Power	a	R^2
0	0	0.0399	0.9599	2%-3%	0	0.0357	0.9233
	20	0.0389	0.9761		20	0.0310	0.9788
	30	0.0374	0.9943		30	0.0309	0.9897
	40	0.0372	0.9847		40	0.0290	0.9879
	50	0.0365	0.9629		50	0.0287	0.9696
3%-4%	0	0.0326	0.9408	4%-5%	0	0.0319	0.9662
	20	0.0300	0.983		20	0.0282	0.990
	30	0.0285	0.9894		30	0.0270	0.9863
	40	0.0280	0.9742		40	0.0264	0.990
	50	0.0278	0.9699		50	0.0258	0.9845

desorption more sensitive to pressure. The sensitivity of desorption to pressure on the right side of the intersection is mainly caused by the cracking induced by infrared radiation. When the pressure is high, the coal matrix gets compressed, and temperature differences at different positions of the coal rock generate a tearing effect that increases internal fractures in the channel.

- 4) In light of the influence of the power of infrared radiation and moisture, the classical Langmuir model of isothermal adsorption was modified to analyze the parameter of maximum adsorption. As the power of infrared radiation and the moisture content increase, gradually reduces, which is consistent with the experimental results and confirms the accuracy of the improved model. A model of the heating of the coal rock under the action of infrared radiation was constructed by combining experimentation and theory. Both the models of adsorption and heating provide a theoretical reference for mining coalbed methane using infrared radiation.

Acknowledgements

Supported by the Scientific Research Project (Surface Project) of Liaoning Provincial Department of Education (Nos. LJK20329 and LJK20360). The Liaoning Province Applied Basic Research Program (Nos. 2022JH2/101300136).

Conflict of interest

The authors declare no competing interest.

Open Access This article is distributed under the terms and conditions of the Creative Commons Attribution (CC BY-NC-ND) license, which permits unrestricted use, distribution, and reproduction in any medium, provided the original work is properly cited.

References

- Avner, V., Robert, B. J., Nathaniel, W., et al. A critical review of the risks to water resources from unconventional shale gas development and hydraulic fracturing in the United States. *Environmental Science & Technology*, 2014, 48(15): 8334-8348.
- Aylin, Ç. K., Tayfun, B. Forecasting of CO₂ emissions from fuel combustion using trend analysis. *Renewable and Sustainable Energy Reviews*, 2010, 14(9): 2906-2915.
- Boleslav, T. Flow calorimetric insight to competitive sorption of carbon dioxide and methane on coal. *Thermochimica Acta*, 2011, 523(1): 250-252.
- Cai, J. W., Yang, S. Q., Hu, X. C., et al. Risk assessment of dynamic disasters induced by gas injection displacement in coal seams. *Process Safety and Environmental Protection*, 2019, 128: 41-49.
- Chen, Y., Fu, H. Y., Ma, D. M., et al. Differences of the pore structure and methane adsorption/desorption between vitrain and durain of low-rank coals: Case study in the Huanglong Coalfield, southern Ordos Basin, China. *Journal of Energy Engineering*, 2021, 147(5): 04021038.
- Chen, D., Pan, Z. J., Liu, J. S., et al. Modeling and simulation of moisture effect on gas storage and transport in coal seams. *Energy & Fuels*, 2012, 26(3): 1695-1706.
- Fan, Z. L., Fan, G. W., Zhang, D. S., et al. Optimal injection timing and gas mixture proportion for enhancing coalbed methane recovery. *Energy*, 2021, 222: 119880.
- Feng, Y. Y., Zhang, L. X. Scenario analysis of urban energy saving and carbon abatement policies: A case study of Beijing city, China. *Procedia Environmental Sciences*, 2012, 13: 632-644.
- Guo, H. G., Zhang, Y. J., Zhang, Y. W., et al. Feasibility study of enhanced biogenic coalbed methane production by super-critical CO₂ extraction. *Energy*, 2021a, 214: 118935.
- Guo, Z. X., Zhao, J. Z., You, Z. J., et al. Prediction of coalbed methane production based on deep learning. *Energy*, 2021b, 230: 120847.
- Jamil, A., Umer, S., Rabia, R., et al. Microwave chemistry: Effect of ions on dielectric heating in microwave ovens. *Arabian Journal of Chemistry*, 2015, 8: 100-104.
- Krooss, B. M., Bergen, F. V., Gensterblum, Y., et al. High-pressure methane and carbon dioxide adsorption on dry and moisture-equilibrated Pennsylvanian coals. *International Journal of Coal Geology*, 2002, 51(2): 69-92.
- Laith, A. N., Salim, H. J., Mohammed, J. Y., et al. Modification of Langmuir model for simulating initial pH and temperature effects on sorption process. *Separation Science and Technology*, 2020, 55(15): 2729-2736.
- Lan, W. J., Wang, H. X., Zhang, X., et al. Investigation on the mechanism of micro-cracks generated by microwave heating in coal and rock. *Energy*, 2020, 206: 118211.
- Längauer, M., Zitzenbacher, G., Burgstaller, C., et al. Enhanced infrared heating of thermoplastic composite sheets for thermoforming processes. *International Polymer Processing*, 2021, 36(1): 35-43.
- Lin, D., Wang, J., Yuan, B., et al. Review on gas flow and recovery in unconventional porous rocks. *Advances in Geo-Energy Research*, 2017, 1(1): 39-53.
- Liu, J., Kang, Y. L., Chen, M. J., et al. Effect of high-temperature treatment on the desorption efficiency of gas in coalbed methane reservoirs: Implication for formation heat treatment. *International Journal of Hydrogen Energy*, 2022, 47(19): 10531-10546.
- Liu, X. J., Zhang, X., Wen, Q. Z., et al. Experimental research on the proppant transport behavior in nonviscous and viscous fluids. *Energy & Fuels*, 2020, 34(12): 15969-15982.
- Lu, Y. Y., Zhang, H. D., Zhou, Z., et al. Current status and effective suggestions for efficient exploitation of coalbed methane in China: A review. *Energy & Fuels*, 2021, 35(11): 9102-9123.
- Noboru, S., Tamotsu, H. Applications and advances in far-infrared heating in Japan. *Trends in Food Science & Technology*, 1994, 5(11): 357-362.
- Qin, X., Singh, H., Cai, J. Sorption characteristics in coal and shale: A review for enhanced methane recovery. *Capillarity*, 2022, 5(1): 1-11.
- Qu, H. Y., Liu, J. S., Chen, Z. W., et al. Complex evolution of coal permeability during CO₂ injection under variable temperatures. *International Journal of Greenhouse Gas Control*, 2012, 9: 281-293.

- Salam, A. A., Ammar, B. A., Asaad, R. S., et al. A comprehensive review on infrared heating applications in food processing. *Molecules*, 2019, 24(22): 4125.
- Sang, S. X., Xu, H. J., Fang, L. C., et al. Stress relief coalbed methane drainage by surface vertical wells in China. *International Journal of Coal Geology*, 2010, 82(3): 196-203.
- Song, K. L., Yao, L. Study on the characteristics of coalbed methane composition and main geological controlling factors in FUXIN basin. *Fresenius Environmental Bulletin*, 2022, 31(8): 7967-7974.
- Stefan, O., Ronny, P., Giuseppe, S., et al. Competitive adsorption equilibria of CO₂ and CH₄ on a dry coal. *Adsorption*, 2008, 14: 539-556.
- Su, X. Y., Feng, Z. C., Cai, T. T., et al. Coal permeability variation during the heating process considering thermal expansion and desorption shrinkage. *Adsorption Science & Technology*, 2022, 2022: 7848388.
- Teng, T., Gao, F., Ju, Y., et al. How moisture loss affects coal porosity and permeability during gas recovery in wet reservoirs? *International Journal of Mining Science and Technology*, 2017, 27(6): 899-906.
- Teng, T., Wang, J. G., Gao, F., et al. Complex thermal coal-gas interactions in heat injection enhanced CBM recovery. *Journal of Natural Gas Science and Engineering*, 2016, 34: 1174-1190.
- Tomone, A., Yoshio, H., Kanichi, S. Heat transfer characteristics of superheated steam combined with far infrared heating. *Food Science and Technology Research*, 2005, 11(4): 363-368.
- Wang, Z. F., Su, W. W., Tang, X., et al. Influence of water invasion on methane adsorption behavior in coal. *International Journal of Coal Geology*, 2018, 197: 74-83.
- Wang, W. L., Zhao, C., Sun, J., et al. Quantitative measurement of energy utilization efficiency and study of influence factors in typical microwave heating process. *Energy*, 2015, 87: 678-685.
- Xu, X. T., Shao, L. Y., Fu, Y. F., et al. Sequence palaeogeography, lacustrine basin evolution, and coal accumulation in the lower cretaceous Fuxin continental faulted basin, China. *Geological Journal*, 2020, 55(2): 1195-1215.
- Yan, Q. Y., Christina, L., Zuleima, T. K., et al. Experimental investigation of shale gas production impairment due to fracturing fluid migration during shut-in time. *Journal of Natural Gas Science and Engineering*, 2015, 24: 99-105.
- Ye, Z. H., Chen, D., Pan, Z. J., et al. An improved Langmuir model for evaluating methane adsorption capacity in shale under various pressures and temperatures. *Journal of Natural Gas Science and Engineering*, 2016, 31: 658-680.
- Ye, D., Liu, G., Gao, F., et al. A multi-field coupling model of gas flow in fractured coal seam. *Advances in Geo-Energy Research*, 2021, 5(1): 104-118.
- Yu, F. H., Hsuan, T. S., Pei, T. C. Co-torrefaction of sewage sludge and leucaena by using microwave heating. *Energy*, 2016, 116: 1-7.